



## Enhancement and mechanism of electrochemical degradation of pyridine contaminated wastewater

Lijing Xue<sup>a</sup>, Weiwu Hu<sup>a,b,\*</sup>, Chuanping Feng<sup>a</sup>, Nan Chen<sup>a</sup>, Hongyan Chen<sup>c</sup>, Zhengxia Hu<sup>a</sup>

<sup>a</sup>School of Water Resources and Environment, MOE Key Laboratory of Groundwater Circulation and Environmental Evolution, China University of Geosciences (Beijing), Beijing 100083, China, Tel. +86 10 82322281; Fax: +86 10 82321081; email: 2007012116@cugb.edu.cn (W. Hu), 1732696149@qq.com (L. Xue), fengcp@cugb.edu.cn (C. Feng), chennan@cugb.edu.cn (N. Chen), chybo1999@163.com (H. Chen), 1131626295@qq.com (Z. Hu)

<sup>b</sup>The Journal Center, China University of Geosciences (Beijing), Beijing 100083, China

<sup>c</sup>School of Science, Beijing Forestry University, Beijing 100083, China

Received 11 April 2019; Accepted 1 January 2020

### ABSTRACT

Pyridine is an emerging contaminant in groundwater which can adversely affect human health and the electrochemical method has been a paramount method to address it. The present study investigated the degradation of pyridine with Ti/RuO<sub>2</sub> anode and Cu-Zn cathode which were combined with a wire entanglement in an undivided catalysis cell, and the system was enhanced by an iron net. First, the enhancement of iron net on electrochemical degradation of pyridine was studied by comparing the presence and absence of iron net. Then, the influencing factors of the electro-iron system, including current density, NaCl dosage and plate distance was studied and Box–Behnken design was employed to investigate the interaction of the three parameters (current density, plate distance, and supporting electrolyte dosage) on the removal of pyridine. Moreover, the electrochemical enhanced pyridine degradation mechanism by iron net was analyzed with cyclic voltammetry (CV) analysis. The reaction pathway and intermediates of pyridine oxidation were also described. It was found that the degradation efficiency of pyridine in the electrochemical system could be increased by 11.3% by adding an iron net. Based on the response surface methodology analysis, the pyridine removal efficiency of 90.2% was achieved under the optimal conditions with a current density of 99.45 mA cm<sup>-2</sup>, plate distance of 2.99 cm and NaCl dosage of 8.78 g L<sup>-1</sup>. The CV curve found that the electrochemical oxidation of pyridine was accomplished by indirect oxidation. Pyridine reacts with the oxide formed by Cl<sup>-</sup> to form intermediates of small organic acid, which can be further mineralized to be CO<sub>2</sub> and H<sub>2</sub>O. Adding an iron net can reduce hydrogen by electrochemical corrosion and reduce the carbonyl group of the intermediate product to hydroxyl group, thereby promoting the degradation of pyridine. This study provides a potentially efficient method for disposing of wastewater pollution caused by pyridine.

**Keyword:** Electrochemical oxidation; Enhancement; Optimization; Box–Behnken design (BBD); Response surface methodology (RSM)

### 1. Introduction

Pyridine, a typical nitrogen-containing heterocyclic compound, is commonly used as a raw material or intermediate in the agrochemical and pharmaceutical industries,

including synthetic vitamins, sulphonamides, disinfectant products, dyes, explosives, rubber and paint [1,2]. Discharges from agricultural and industrial production lead to the presence of pyridine in groundwater [3]. Pyridine poses a huge

\* Corresponding author.

threat to human health because of its toxicity, and its high concentration in drinking water can cause teratogenic in humans and animals [4,5]. In the U.S., pyridine is classified as a hazardous substance and has been listed as a priority pollutant by the U.S. Environmental Protection Agency (USEPA) [6,7]. In China, the annual production of pyridine reaches 114,000 t, which has a serious impact on human health [8]. Therefore, it is essential to investigate the pyridine removal technology in groundwater.

To date, various types of technologies, such as photo-synthetic degradation [9,10], biological treatment [11,12], photoelectrocatalysis [13], microwave process [14], Fenton reagent [15,16], adsorption [17] and electrochemical oxidation [18], have been used to deal with pyridine pollution. Among them, electrochemical oxidation has been increasingly recognized as a promising method for remediation of groundwater contaminated with pyridine due to its mild reaction condition, high reaction rate and stable oxidation ability [19,20]. Electrode material plays an important role in electrochemical oxidation process, it had been reported that when 200 g L<sup>-1</sup> pyridine was electrolyzed by a tin oxide tubular ceramic membrane electrode under the conditions of 10 g L<sup>-1</sup> Na<sub>2</sub>SO<sub>4</sub> and 25 mA cm<sup>-2</sup>, the removal efficiency of pyridine can reach 70.1%, but the electrode had a higher cost and shorter life [18]. Ti/RuO<sub>2</sub> has been extensively applied as a representative electrode material owing to its high electrocatalytic activity and corrosion resistance in chloride-containing solutions in recent years [21,22]. However, the disadvantages of electrochemical oxidation with Ti/RuO<sub>2</sub>, such as high energy consumption and low current efficiency, have great constraints on its practical application [23]. It has been reported that the addition of iron net was conducive to the degradation of nitrate in wastewater, and higher nitrate reduction efficiency of 90.1% and lower energy consumption were obtained by introducing three pieces of the iron net between electrodes [24]. Moreover, a novel electrochemical system for the establishment of a boron-doped diamond anode and a carbon felt cathode was constructed to degrade wastewater containing p-nitrophenol and a built-in iron electrode between anode and cathode, the degradation efficiency was significantly enhanced by iron electrode [25]. However, few investigations are presently available for iron net enhanced electrochemical degradation of pyridine. Still, it is not clear that the effects of different factors on the electrochemical degradation of pyridine enhanced by the iron net, and the reinforcement mechanism of the iron net remain unknown.

Herein, the influence of different factors (e.g. current density, plate distance and supporting electrolyte dosage) on pyridine removal was investigated by using a laboratory-scale iron net enhanced electrocatalytic reactor. Box-Behnken design (BBD) was chosen to investigate the interaction of three parameters (current density, plate distance, and supporting electrolyte dosage) on the removal of pyridine, and response surface methodology (RSM) was used to describe the mathematical relationship between the response function and these factors. Moreover, the oxidation type and degradation mechanism of electrochemical pyridine enhanced by iron net were analyzed by using cyclic voltammetry (CV) analysis. This study offers the optimal conditions for the removal of pyridine in the iron net enhanced electrochemical

oxidation system and is of great significance to the practical remediation of pyridine pollution.

## 2. Experimental setup

### 2.1. Experimental apparatuses and materials

A 653 mL cylinder acrylic cell was constructed (Fig. 1), with a working volume of 500 mL. The cathode made of Ti/RuO<sub>2</sub> (Shuangyang, Beijing, China) and the anode made of Cu-Zn (Cu-Zn, 59/41 wt.%) (Shuangyang, Beijing, China) with a side plate of 51.6 cm<sup>2</sup> (43 mm × 120 mm × 1 mm) constituted an electrochemical reaction device. An iron net (43 mm × 120 mm × 1 mm) was placed in the middle of the two electrodes to enhance the electrochemical degradation of pyridine. A continuous magnetic stirrer in the cell bottom was used to increase the turbulence of the solution. A DC power supply (KXN-645D, Zhaoxin, China) with a voltage range of 0–50 V and a current range of 0–5 A were employed to provide a constant current.

Synthetic wastewater with a target concentration of 100 mg L<sup>-1</sup> (pyridine) was prepared with deionized water and NaCl was added to increase the conductivity of the electrolyte at initial pH of 7.8. All chemical reagents were of analytical grade in this study (Sinopharm, China).

### 2.2. Batch experiment

A 500 mL synthetic wastewater was added to the cylinder acrylic cell and the Cu-Zn cathode was burnished with sandpaper (600 mesh) before electrolysis to remove the oxide layer. The comparative experiments with and without adding iron net were carried out under the conditions of pyridine concentration of 100 mg L<sup>-1</sup>, current density of 60 mA cm<sup>-2</sup>, plate distance of 2 cm, NaCl of 10 g L<sup>-1</sup> and pH of 7.8 to study the enhancement of iron net on the electrochemical degradation of pyridine. The current density was set at 20, 60 and 100 mA cm<sup>-2</sup> to investigate its effect on pyridine removal. Since the pyridine is mainly derived from pharmaceutical wastewater and some fine chemical industries, the production wastewater of the manufacturing process tends to have a high salinity of more than 10 g L<sup>-1</sup> in particular [26], the NaCl dosages was set at 5, 10 and 15 g L<sup>-1</sup> to investigate its effect on pyridine removal. For the same purpose, the plate distance was set at 1.0, 2.0 and 3.0 cm. 4.5 mL sample was extracted from electrochemical cell for analysis at

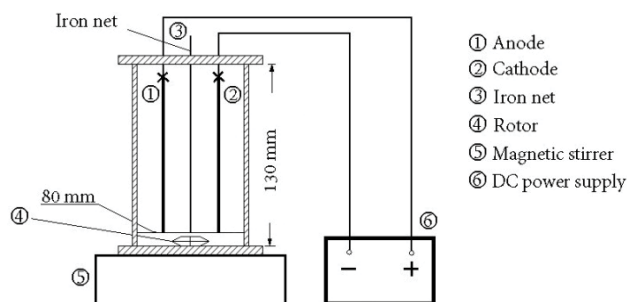


Fig. 1. Schematic diagram of the electrocatalytic reactor system.

different time intervals. All experiments were conducted at room temperature ( $25^{\circ}\text{C} \pm 2^{\circ}\text{C}$ ).

### 2.3. Analytical methods

The surface morphology of the Ti/RuO<sub>2</sub> electrode was characterized with a scanning electron microscopy (SEM, JEOL JSM-6480LV, Japan). The CV curve of the Ti/RuO<sub>2</sub> electrode was measured by the electrochemical workstation (CHI660D, Chenhua, China). The Ti/RuO<sub>2</sub> electrode was employed as the working electrode, meanwhile the Cu-Zn electrode was used as the counter electrode, and the Ag/AgCl/0.3 M KCl was served as the reference electrode. pH value was determined by using a pH/ORP meter (AS-211, Twin, Japan).

The concentration of pyridine was determined by the high-performance liquid chromatography (HPLC) (1260 infinity, Agilent, USA), which was equipped with a XDB-C18 column (4.6 mm × 250 mm, 5 μm) [27]. The mobile phase consisted of methanol (70%, volume percent) was adjusted to pH 2.5 with dilute phosphoric acid (30%, volume percent). The injection volume of the sample was set to 20 μL with the flow rate of 1.0 mL min<sup>-1</sup>, and the room temperature was regarded as the column temperature ( $25^{\circ}\text{C} \pm 0.2^{\circ}\text{C}$ ). These chromatographic conditions were employed to test pyridine at detection wavelength 540 nm.

### 2.4. Experimental design and statistical analysis

Experimental design, mathematical modeling, and optimization were performed using the design-expert 8.06 software. BBD is recognized as a more effective and ideal method to central composite design because BBD requires fewer experiments, less time and lower cost to build the model equation [28]. Through experimental design and data analysis, BBD allows to calculate the intermediate level of response function and estimate experimental performance at experimental points within the scope of the study [29].

In the present study, BBD was selected to investigate the influences of the three independent variables on electrochemical oxidation of pyridine and to determine the optimal conditions for maximizing the removal efficiency of pyridine. The three independent variables were current density ( $X_1$ ), plate distance ( $X_2$ ), and NaCl dosage ( $X_3$ ) and the corresponding levels were designed as -1, 0, and +1, as shown in Table 1. The objective function was the ratio of pyridine concentration at time  $t$  and initial ( $C_t/C_0$ ). To investigate the electrolysis reaction rate, the pseudo-first-order kinetic model was used to interpret the experimental data.

## 3. Results and discussion

### 3.1. Iron net enhanced electrochemical degradation of pyridine

The Ti/RuO<sub>2</sub> electrode was used as the anode, and the removal efficiency of pyridine was compared with and without the addition of iron net. Fig. 2 shows that the removal efficiency of pyridine reached 56.6% after 240 min of electrolysis without iron net, and the removal efficiency of pyridine was significantly improved to reach 67.9% after adding the iron net. The results showed that the removal of pyridine by the electrochemical system was improved by 11.3% with the

Table 1  
Independent factors and coded levels

Factors	Range and levels		
Coded levels	-1	0	1
Current density, $I$ (mA cm <sup>-2</sup> )	20	60	100
Plate distances, $S$ (cm)	1	2	3
NaCl dosage, $W$ (g L <sup>-1</sup> )	5	10	15

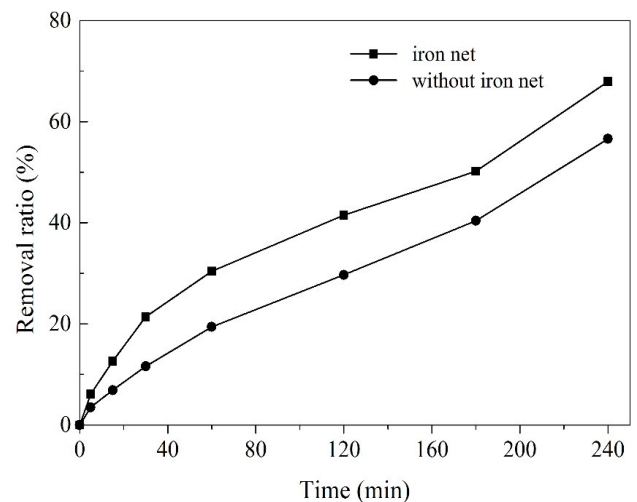


Fig. 2. Effect of iron net on the removal of pyridine.

addition of iron net. It can be seen that the addition of iron net can improve the removal efficiency of pyridine for the forming of a galvanic cell in the system.

When iron net acted as an anode, a corrosion reaction occurred:



When iron net acted as a cathode, a reduction reaction occurred:



In addition, H<sub>2</sub>O<sub>2</sub> and Fe<sup>2+</sup> can form Fenton reagent, and the reactions were:



The addition of iron net enhanced the oxidation and reduction capacity of the electrochemical system, which was mainly based on the oxidation–reduction potential difference between zero valence iron and cathode to form the galvanic cell and generate the transfer of charged ions. There were at least two simultaneous reactions on the surface of iron, including a dissolution oxidation reaction as an anode and a reduction reaction as an oxidant [30].

### 3.2. Influence of current density

Applying current density is a key parameter for electrochemical processes, because it can affect the electrochemical oxidation process by regulating the hydroxyl radical generation capacity on the electrode surface [31]. To evaluate the effect of current density, a series of experiments with different current densities ranged from 20 to 100 mA cm<sup>-2</sup> with initial pyridine concentration of 100 mg L<sup>-1</sup>, pH of 7.8 and NaCl dosage of 10 g L<sup>-1</sup> were conducted. It can be seen that the increase of current density had a significant effect on the electrochemical degradation of pyridine in Fig. 3. With the increase of current density from 20 to 100 mA cm<sup>-2</sup>, the removal efficiency of pyridine increased from 39.4% to 90.2%. This phenomenon was attributed to the high transfer rate of electron and the increased formation rate of strong oxidation materials (e.g.  $\cdot\text{OH}$ ,  $\text{H}_2\text{O}_2$ ) between pyridine and electrodes at higher current densities [32]. However, the decrease of pyridine did not change linearly with the increase of current density, due to the large power consumption by the side reaction of oxygen evolution [33], which was shown in Eq. (5) [34]:



Fig. 3 shows the non-linear regression of pyridine concentration with electrochemical oxidation time and confirmed a pseudo-first-order kinetic model. Table 2 lists the  $k$  and  $r^2$  values for each group of experiment. The apparent rate constant ( $k_{\text{app}}$ ) of pyridine removal increased as the current density increased from 0.00208 min<sup>-1</sup> at 20 mA cm<sup>-2</sup>, 0.00431 min<sup>-1</sup> at 60 mA cm<sup>-2</sup> to 0.00682 min<sup>-1</sup> at 100 mA cm<sup>-2</sup>, respectively. However, it has been confirmed in previous studies that large applied currents can reduce the current efficiency of electrochemical oxidation process and result in high operating costs [35,36]. Therefore, a larger current density can achieve better results considering the removal efficiency of pyridine, but it is not suitable for practical use in terms of cost analysis.

### 3.3. Influence of NaCl dosage

In this work, NaCl was chosen as a supporting electrolyte to enhance the solution conductivity, because it is more easily available at the production site [37]. Fig. 4 shows the influence of different NaCl dosages on pyridine removal in electrochemical system with a pH of 7.8 and a current density of 60 mA cm<sup>-2</sup>. After 240 min of electrolysis, it can be found that the pyridine concentration decreased from 100 to 54.92, 50.35 and 45.13 mg L<sup>-1</sup> at the NaCl dosages of 5, 10 and 15 g L<sup>-1</sup>, respectively. Increasing the concentration of supporting electrolyte had a positive influence on the pyridine removal efficiency with the NaCl addition in the range of 5–10 g L<sup>-1</sup>. These explanations can be given by the evolutionary reaction of chlorine [38]. The existing of chloride ions not only enhanced the conductivity of the solution, but also generated a series of active intermediates during the electrochemical oxidation process (Eqs. (6)–(9)). In fact, the formation process of available chlorine can be considered as two processes. Firstly, chloride ion was converted into chlorine gas on the surface of Ti/RuO<sub>2</sub> anode. Secondly, the

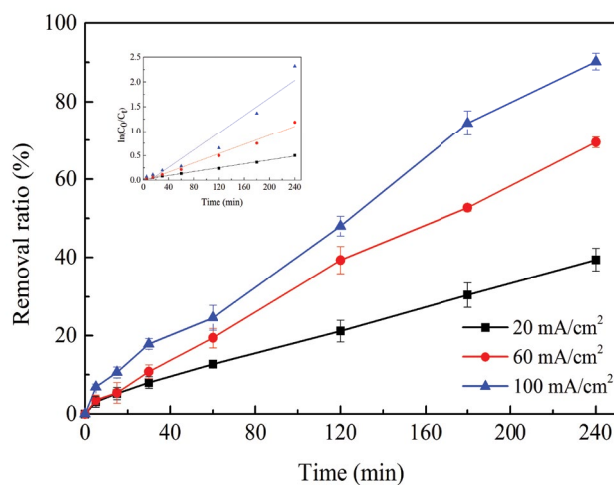


Fig. 3. Removal ratio of pyridine changes as a function of electrolysis time at different current densities, 10 g L<sup>-1</sup> of NaCl, 3 cm plate of distance.

Table 2  
Influence of current density, NaCl dosage, initial pH and plate distance on pseudo-first-order  $k$  and  $r^2$  values for electrochemical degradation pyridine

Influence of current density		
Current density (mA cm <sup>-2</sup> )	$k$ ( $\times 10^{-2}$ min <sup>-1</sup> )	$r^2$
20	0.208	0.9890
60	0.431	0.9906
100	0.682	0.9664
Influence of NaCl		
Concentration of NaCl (g L <sup>-1</sup> )	$k$ ( $\times 10^{-2}$ min <sup>-1</sup> )	$r^2$
5	0.256	0.9868
10	0.276	0.9878
15	0.326	0.9907
Influence of plate distance		
Plate distance (cm)	$k$ ( $\times 10^{-2}$ min <sup>-1</sup> )	$r^2$
1	0.180	0.9864
2	0.337	0.9965
3	0.472	0.9949

generated chlorine gas was immediately reacted with water and promoted the formation of hypochlorous acid/hypochlorite [39]. Based on the previous studies [40,41], some other reactions of chloride on the surface of anode are given in Eqs. (10) and (11) [42,43]. A consistent conclusion was also reached in the electrochemical reduction of nitrate [24].



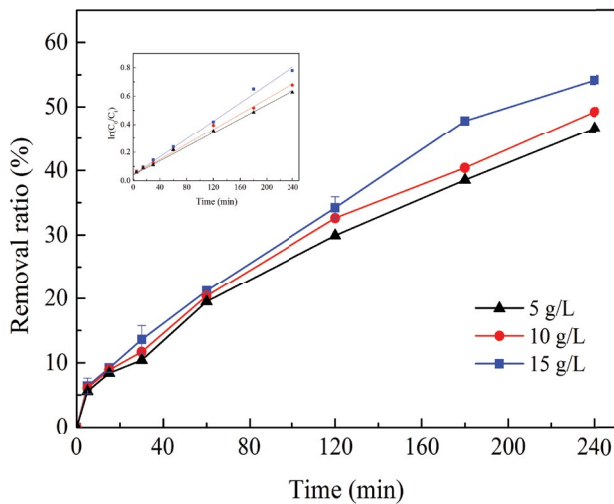
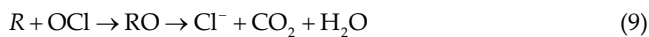


Fig. 4. Removal ratio of pyridine changes as a function of electrolysis time at different NaCl dosages, 60 mA cm<sup>-2</sup> of current density, 2 cm of plate distance.



However, it can be seen from the experimental results that the NaCl dosage had little effect on the removal of pyridine. Moreover, it also indicated that the pyridine degradation at different NaCl dosages was consistent with the pseudo-first-order equation. The  $k$  and  $r^2$  values of the experiment in each group are depicted in Table 2, in which it can be inferred that  $k_{app}$  value was very close when the NaCl dosage was 5, 10 and 15 g L<sup>-1</sup>, respectively. This can be due to the fact that the excessive salinity might lead to a greater amount of Cl<sup>-</sup> adsorbed on the anode surface and a minimizing number of active sites on the electrode [18]. In fact, previous study had confirmed that the chloroform was the main by-product during electrochemical treatment process of organic matter with the presence of chloride ions [44]. In practical application, the integration of different processes was necessary for harmless treatment of this wastewater. Fortunately, it had been proved that the organochlorine by-products such as chloroform can be efficient adsorbed by activated carbon, which provided a feasible alternative for the separation of organochlorine from solution [45]. Therefore, the integration of electrochemical oxidation process and activated carbon adsorption process provided a feasible method for the efficient and harmless treatment of pyridine as well as its by-products. In addition, considering the problem of high concentration of NaCl, in fact, pyridine wastewater was mainly produced from pharmaceutical wastewater and some fine chemical industries. Due to the high toxicity of pyridine, electrochemical oxidation process was often used as a pretreatment process before the sewage enters the aerobic biological reactor. At present, the salinity

can be separated after electrolysis using desalination process (such as MVR process and high-efficiency evaporation process [46]).

### 3.4. Influence of plate distance

The effect of plate distance between two electrodes on the removal behavior of pyridine was investigated at different plate distance of 1, 2 and 3 cm at current density of 60 mA cm<sup>-2</sup>, NaCl dosage of 10 g L<sup>-1</sup> and pH of 7.8. The removal efficiency of pyridine was 34.7%, 53.9% and 69.7% at plate distance of 1, 2 and 3 cm, respectively (Fig. 5). Fig. 5 also shows that the concentration variation of pyridine with time fitted the pseudo-first-order kinetic model, and the  $k$  and  $r^2$  values were listed in Table 2. As shown in Table 2, the highest  $k$  value (0.00472 min<sup>-1</sup>) was obtained at 3 cm of plate distance, and the  $k$  value of 0.00180 and 0.00337 min<sup>-1</sup> was obtained at 1 and 2 cm of plate distance, respectively. It was worth noting that when the plate distance was 3 cm, the removal efficiency of pyridine was 69.7%, which was a twice time higher than that at plate distance of 1 cm. There might be two possible reasons: (1) the mass transfer process would become a limiting factor for the overall reaction kinetics when the applied current density exceeded the limiting current density of electrochemical oxidation [47,48], the contaminants need to migrate to the middle of two poles first and then the oxidation reaction was realized by the contacting of anode surface in direct oxidation process, therefore the decreasing plate distance resulted in reducing the effective mass transfer volume between the plates [49]; (2) a small plate distance was conducive to corrosion oxidation of the electrode, which will consume the current and cause the electrode passivation [50]. Although the anode potential was lowered when the plate distance was reduced under the same conditions and thereby reducing the energy consumption, smaller plate distance still cannot be applied in practical engineering considering the effects of the mass transfer process.

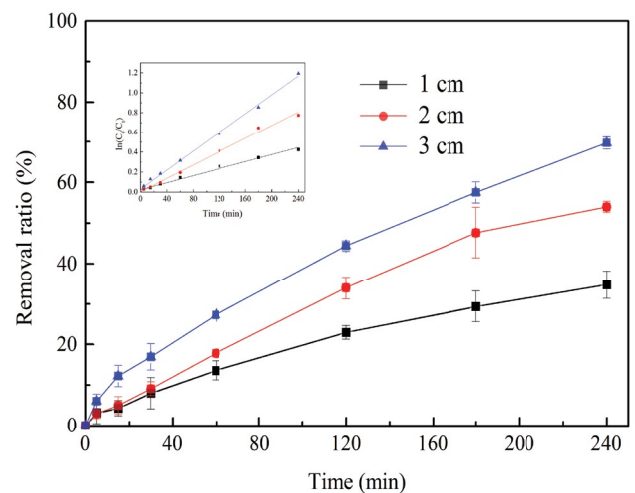


Fig. 5. Removal ratio of pyridine changes as a function of electrolysis time at different plate distance, 60 mA cm<sup>-2</sup> of current density, 10 g L<sup>-1</sup> of NaCl.

3.5. BBD optimization

According to the BBD design, 17 groups of experiments were implemented, and the data are listed in Table 3. The BBD has a processing combination at the midpoint of the edge of the test space and does not contain an embedding factor or partial factorial design [29].

The application of RSM offers an empirical relationship between function and the independent variables [38]. A quadratic polynomial equation was given, which can be approximated to describe the mathematical relationship between the response function (Y) and the independent variables (X) as the following Eq. (12):

$$Y = 0.5 - 0.24X_1 - 0.14X_2 - 0.023X_3 - 0.033X_1X_2 + 0.010X_1X_3 + 0.010X_2X_3 + 0.035X_1^2 - 0.012X_2^2 - 0.018X_3^2 \quad [12]$$

Based on the coefficient in Eq. (8), it can be observed that the degradation rate of pyridine concentration at *t* and initial *t* ( $C_t/C_0$ ) decreased with current density ( $X_1$ ), plate distance ( $X_2$ ) and NaCl dosage ( $X_3$ ). The current density played a more important role in electrochemical process of pyridine compared with the plate distance ( $X_2$ ) and NaCl dosage ( $X_3$ ).

The analysis of variance (ANOVA) test (Table 4) showed good conformity, and the predictions of the response function were in good agreement with the experimental data (the relative error was 0.001). The coefficient of Eq. (11) was determined by applying *t*-test and *p*-value. The *p*-value reflects the conformity of the coefficient, which implies that it is significant if  $p < 0.05$  [51]. The linear influences of coefficients  $X_1$ ,  $X_2$  and  $X_3$ , that is current density ( $p < 0.0001$ ), plate distance ( $p < 0.0001$ ) and NaCl dosage ( $p < 0.0001$ ) were significant. Similarly, the interactive effects of current density and plate distance ( $p < 0.0001$ ), current density and NaCl dosage ( $p < 0.0001$ ), plate distance and NaCl dosage ( $p < 0.0153$ ) were also significant. The *p*-values of the quadratic terms that are current density ( $X$ ) ( $p < 0.0001$ ), plate distance ( $X$ ) ( $p < 0.0046$ ) and NaCl dosage ( $X$ ) ( $p < 0.0007$ ) were more significant. ANOVA for response surface quadratic model gave

*F*-value of 1796.61,  $R^2 = 0.9996$  and coefficient of variation (C.V. = 1.25%),  $p < 0.0001$ , signifying that the model was significant and the experiment was highly accurate and reliable (Table 4).

Fig. 6 shows a response surface plot of the relationship of current density, plate distance and NaCl dosage on the removal of pyridine. Design-expert software was chosen to find the optimal conditions for pyridine removal. The main purpose of this study was to maximize the removal efficiency of pyridine by using the desirability functions to calculate all responsibility factors. The duplicate confirmatory experiment was implemented by using the

Table 3  
Results of the observed value of  $C_t/C_0$

Run	Current density (mA cm <sup>-2</sup> )	Plate distances (cm)	NaCl (g L <sup>-1</sup> )	Actual value ( $C_t/C_0$ )
1	60.00	3.00	5.00	0.35
2	60.00	2.00	10.00	0.50
3	100.00	2.00	5.00	0.27
4	60.00	1.00	5.00	0.65
5	60.00	3.00	15.00	0.31
6	100.00	1.00	10.00	0.46
7	100.00	3.00	10.00	0.10
8	20.00	3.00	10.00	0.68
9	60.00	1.00	15.00	0.57
10	60.00	2.00	10.00	0.50
11	20.00	2.00	5.00	0.81
12	20.00	1.00	10.00	0.85
13	60.00	2.00	10.00	0.50
14	100.00	2.00	15.00	0.29
15	20.00	2.00	15.00	0.70
16	60.00	2.00	10.00	0.50
17	60.00	2.00	10.00	0.50

Table 4  
ANOVA test for response function Y

Source	Sum of squares	df	Mean square	F-Value	p-value	Prob > F
Model	0.64	9	0.071	1,796.51	<0.0001	Significant
A - Current density	0.46	1	0.46	11,729.45	<0.0001	
B - Plate distance	0.15	1	0.15	3,780.32	<0.0001	
C - NaCl	5.513E-003	1	5.513E-003	140.32	<0.0001	
AB	9.025E-003	1	9.025E-003	229.73	<0.0001	
AC	4.225E-003	1	4.225E-003	107.55	<0.0001	
BC	4.000E-004	1	4.000E-004	10.18	0.0153	
A <sup>2</sup>	5.158E-003	1	5.158E-003	131.29	<0.0001	
B <sup>2</sup>	6.579E-004	1	6.579E-004	16.75	0.0046	
C <sup>2</sup>	1.289E-003	1	1.289E-003	32.82	0.0007	
Residual	2.750E-004	7	2.750E-004			
Lack of fit	2.750E-004	3	2.750E-004	3.48	0.1202	Not significant
Pure error	2.21	4	0.57			
Cor. total	0.64	16				

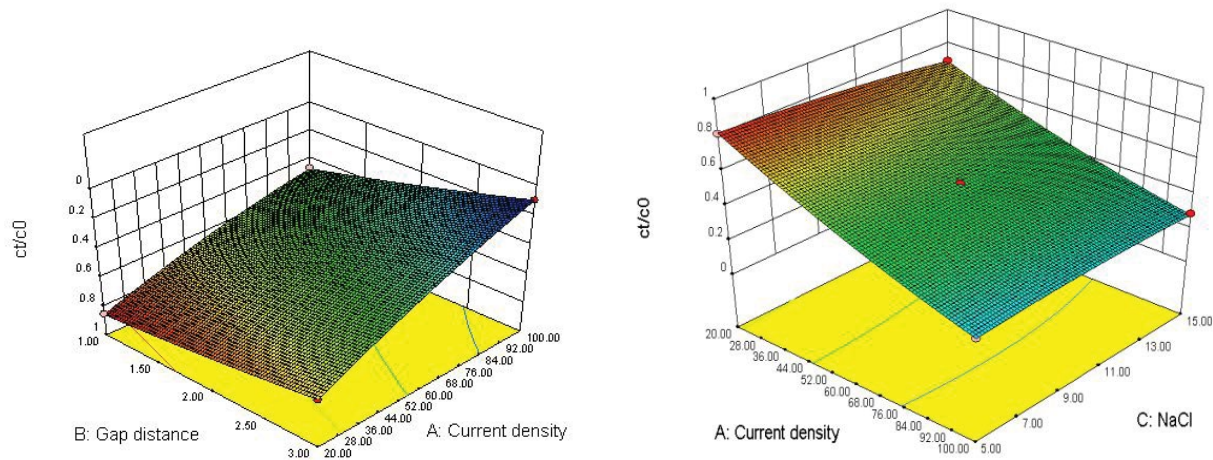


Fig. 6. Three-dimensional response surface plot for (a) influence of current density and plate distance and (b) effect of current density and NaCl dosage on the pyridine removal.

optimized parameters. It was found that the optimal condition of current density, plate distance, and NaCl dosage was  $99.45 \text{ mA cm}^{-2}$ ,  $2.99 \text{ cm}$  and  $8.78 \text{ g L}^{-1}$ , respectively, with a predicted value of  $0.9858 (C_i/C_0)$  compared to the actual value of  $0.9844 (C_i/C_0)$ . The results were closely in agreement with the predicted value obtained from the model. In fact, the effects of the three factors optimized in this study on the reaction efficiency can be summarized as follows: (1) the anodization efficiency was controlled by the applied current [47]; (2) the increasing available chlorine concentration was increased with the increasing amount of NaCl dosage [35]; (3) the increase of plate distance was equivalent to the increasing anode potential under the same current density [52]. Therefore, considering the reasons above, the changing of the three conditions was difficult to obtain an extreme value of the pyridine removal efficiency in the response surface. This behavior was consistent with the result obtained from the similar studies reported in the past [53]. Even so, it can reflect the interaction of current density, NaCl dosage and plate distance on pyridine removal to some extent.

### 3.6. Degradation mechanism of electrochemical pyridine enhanced by iron net

The mechanism of electrochemical oxidation contains direct electrochemical oxidation, which occurs on the surface of an electrode, and indirect electrochemical oxidation, which takes place in the electrolyte solution with strong oxidants produced by electrode [54,55]. The CV curves were recorded to explore the oxidation type and degradation mechanism of the electrochemical oxidation of pyridine. Fig. 7 shows the CV curve obtained for the electrochemical oxidation of pyridine using Ti/RuO<sub>2</sub> as a working electrode and Cu-Zn as the counter electrode, which was measured in  $8.78 \text{ g L}^{-1}$  of NaCl solution with  $100 \text{ mg L}^{-1}$  of pyridine at a scan rate of  $20 \text{ mV s}^{-1}$ . As it can be observed that no additional oxidation peaks were found when pyridine was added to the electrolyte, indicating that no direct electrochemical oxidation occurred. It also can be inferred that the

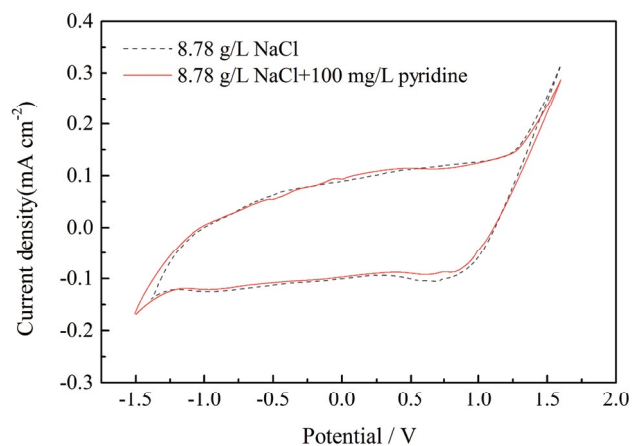


Fig. 7. Cyclic voltammetry obtained in  $8.78 \text{ g L}^{-1}$  of NaCl solution with and without adding  $100 \text{ mg L}^{-1}$  of pyridine.

electrochemical oxidation of pyridine must be accomplished by an indirect oxidation process.

The morphology characteristics of the Ti/RuO<sub>2</sub> electrode surface coatings were obtained by SEM. Fig. 8 shows the SEM microstructures of the original Ti/RuO<sub>2</sub> electrode (Fig. 8a) and the used electrode that sampled from the middle part of the electrode after the experiment (Fig. 8b). It can be observed that the surface of Ti substrate was produced by the pyrolysis oxidation electrode, which usually had a "crack" surface topography. In addition, there was no significant change for Ti electrode surface coatings after the experiment, which indicated that it may have good electrochemical stability.

In order to clarify the pathway of pyridine degradation, HPLC was used to monitor the intermediates during the electrochemical oxidation, and the results are shown in Figs. 9 and 10. It can be found from Fig. 9 that fumaric acid, formic acid, malonic acid and maleic acid were detected by matching with certified reference materials. Furthermore, it also can be seen from Fig. 10 that NO<sub>2</sub> and NO<sub>3</sub> were also

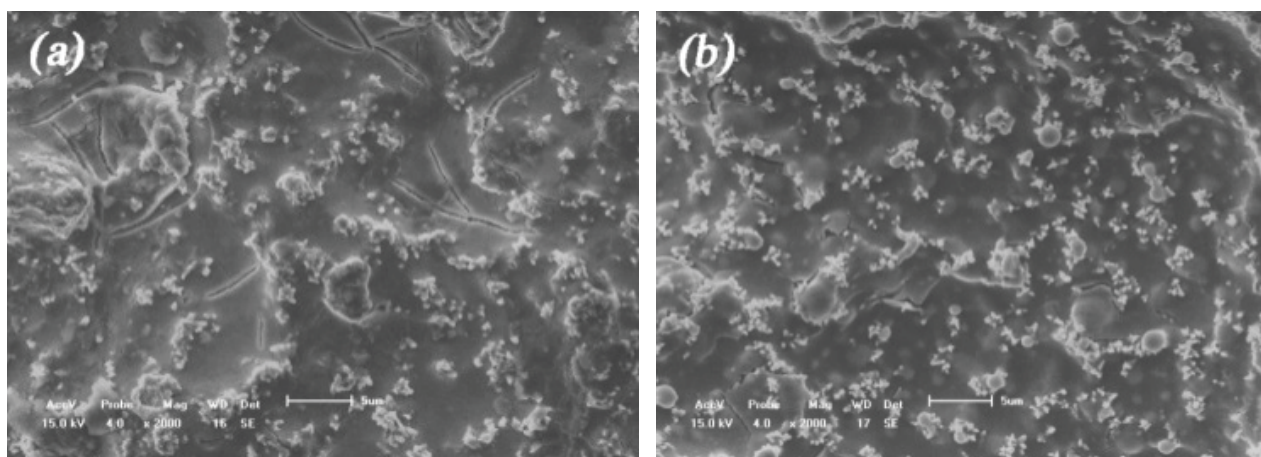


Fig. 8. SEM images of (a) original surface and (b) used (150 h) Ti/RuO<sub>2</sub>.

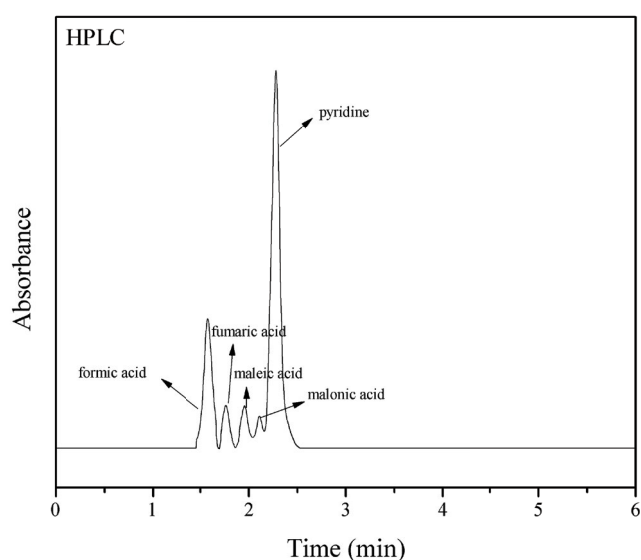


Fig. 9. HPLC maps for matching intermediates for pyridine degradation with certified reference material.

detected in the electrolysis, indicating that the ring-opening reaction of pyridine occurred. Moreover, the almost constant NO<sub>2</sub><sup>-</sup> concentration and gradually increasing NO<sub>3</sub><sup>-</sup> concentration indicated that the occurrence of further oxidation reactions such as NO<sub>2</sub><sup>-</sup> was oxidized to NO<sub>3</sub><sup>-</sup>. The electrochemical degradation products of pyridine were more easily treated by more traditional biological treatment processes than pyridine. Although NaCl had a negative effect on microorganisms, Zhang et al. [56] found that microorganisms can still function at a NaCl concentration of 40 g L<sup>-1</sup>, and the residual NaCl concentration in our experiment was much lower than 40 g L<sup>-1</sup>.

Based on the detected intermediates in the degradation of pyridine, a major electrochemical oxidation pathway was proposed, as shown in Fig. 11. The Ti/RuO<sub>2</sub> electrode can produce a large number of hydroxyl radicals, and the Fenton reaction can produce H<sub>2</sub>O<sub>2</sub> and Cl<sup>-</sup>, then continue to generate HClO, which may attack the pyridine. First, an

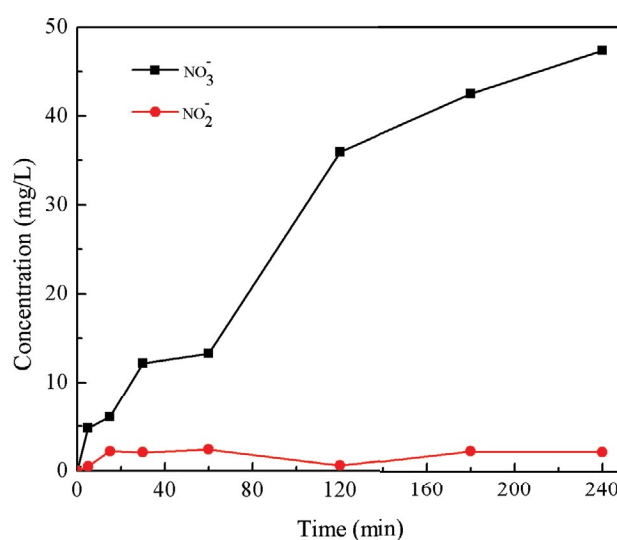


Fig. 10. Concentration variations of NO<sub>2</sub><sup>-</sup> and NO<sub>3</sub><sup>-</sup>.

addition reaction occurs on the pyridine ring to produce pyridin-3-ol. Subsequently, pyridin-3-ol respectively generate pyridin-3,5-diol, pyridin-2,5-diol and pyridin-2,3-diol. After the dehydrogenation reaction, pyridine-2,5-dione, pyridine-3,5(2H,4H) -dione and pyridine-2,3-dione are generated, respectively. Then pyridine-3,5(2H,4H) -dione continues to generate oxalic acid. The pyridine ring undergoes a ring-opening reaction to form formic acid, fumaric acid, maleic acid, malonic acid, NO<sub>2</sub><sup>-</sup> and NO<sub>3</sub><sup>-</sup>. These major by-products were further hydroxylated and the pyridine was finally mineralized into CO<sub>2</sub> and H<sub>2</sub>O. The NO<sub>2</sub><sup>-</sup> was further reduced to N<sub>2</sub> at the cathode.

According to the action mechanism of iron and the detection results of intermediate products mentioned above, the reaction of iron in the system may be caused by the following ways:

- Iron net lost electrons during electrochemical corrosion, and the cathode underwent hydrogen evolution reaction to generate hydrogen with strong reducibility.

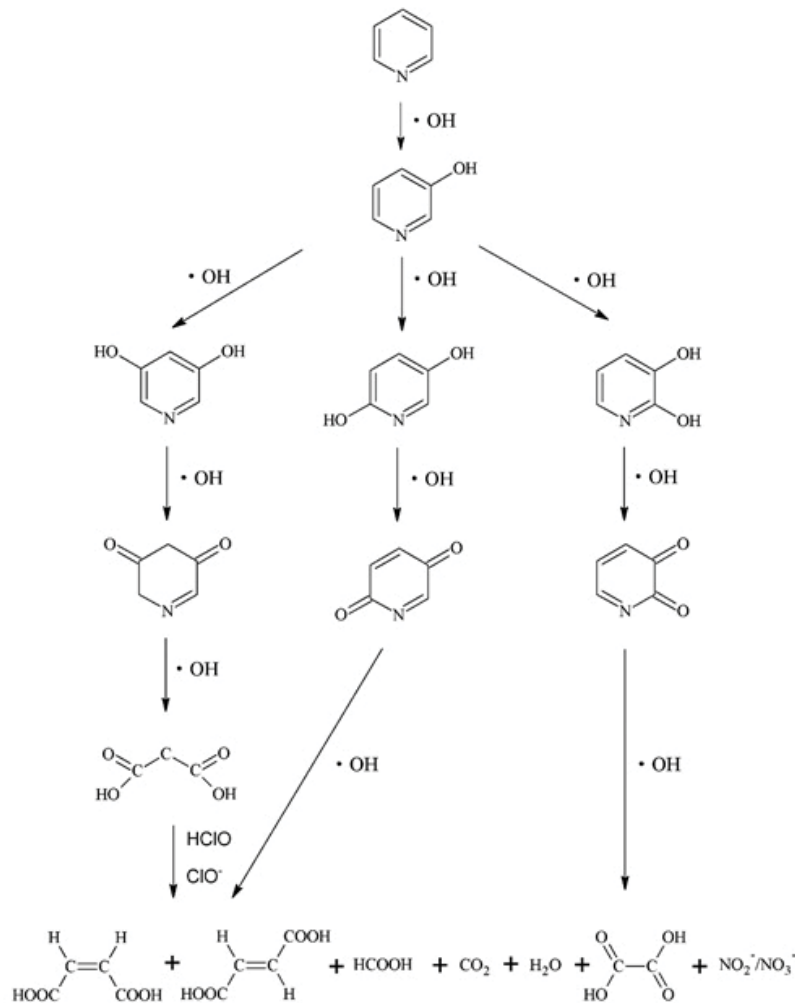


Fig. 11. Proposed pathway for electrochemical degradation of pyridine by Ti/RuO<sub>2</sub> anode and Cu-Zn cathode.



- Then the reductive hydrogen was reduced on the carbonyl group of the intermediate product to form a hydroxyl group.



Therefore, the reduction capacity of the system was enhanced in this process.

#### 4. Conclusions

An electro-iron system for electrochemical oxidation of pyridine removal from contaminated water was constructed and investigated. The influence of different factors on the degradation of pyridine was also evaluated, and numerical optimization of the RSM was chosen to reveal their relationship. The conclusions are drawn as follows:

- Iron net enhanced electrochemical treatment was a more efficient method for pyridine removal than the unreinforced treatment, and the removal efficiency can be improved by 11.3%. The optimal experimental conditions in the present study for maximization removal of pyridine can be obtained by the BBD model. The optimal condition of current density, plate distance, and NaCl dosage was 99.45 mA cm<sup>-2</sup>, 2.99 cm and 8.78 g L<sup>-1</sup>, respectively, at which the pyridine removal efficiency can achieve 98.58%.
- The possible degradation pathway of pyridine was the mineralization process with a small amount of ·OH adsorbed on the surface of the plate. Meanwhile, the pyridine in solution will react with the oxidized Cl<sub>2</sub>, HClO and ClO<sub>2</sub> formed by Cl<sup>-</sup> to produce small molecule organic acids (i.e., maleic acid, fumaric acid, formic acid, and malonic acid). In this process, the pyridinium nitrogen formed NO<sub>2</sub><sup>-</sup>/NO<sub>3</sub><sup>-</sup> and was reduced to N<sub>2</sub> by the action of metallic iron, and the intermediates were further mineralized into CO<sub>2</sub> and H<sub>2</sub>O. The reduced hydrogen produced by the electrochemical corrosion of iron net facilitated the reduction of carbonyl group of the

intermediate product to form a hydroxyl group, thereby promoting the degradation of pyridine.

### Acknowledgment

The authors acknowledge financial support from the National Natural Science Foundation of China (NSFC) (No. 21876159) and the Fundamental Research Fund for the Central Universities (No. 2652018181).

### References

- [1] M. Errami, G.E. Dib, M. Cazaunau, E. Roth, R. Salghi, A. Mellouki, A. Chakir, Atmospheric degradation of pyridine: UV absorption spectrum and reaction with OH radicals and  $O_3$ , *Chem. Phys. Lett.*, 662 (2016) 141–145.
- [2] S. Singh, L.L. Shang, Catalytic performance of hierarchical metal oxides for per-oxidative degradation of pyridine in aqueous solution, *Chem. Eng. J.*, 309 (2016) 753–765.
- [3] Y. Jin, Q. Yue, K. Yang, S. Wu, S. Li, B. Gao, Y. Gao, Pre-treatment of pyridine wastewater by new cathodic-anodic-electrolysis packing, *J. Environ. Sci.*, 63 (2018) 43–49.
- [4] N. Li, X. Lu, S. Zhang, A novel reuse method for waste printed circuit boards as catalyst for wastewater bearing pyridine degradation, *Chem. Eng. J.*, 257 (2014) 253–261.
- [5] J. Wang, X. Jiang, X. Liu, X. Sun, W. Han, J. Li, L. Wang, Microbial degradation mechanism of pyridine by *Paracoccus* sp. NJUST30 newly isolated from aerobic granules, *Chem. Eng. J.*, 344 (2018) 86–94.
- [6] D.H. Lataye, I.M.M. And, I.D. Mall, Removal of pyridine from aqueous solution by adsorption on bagasse fly ash, *Ind. Eng. Chem. Res.*, 45 (2006) 3934–3943.
- [7] F. Tian, R.S. Zhu, K. Song, F. Ouyang, G. Cao, Synergistic photocatalytic degradation of phenol using precious metal supported titanium dioxide with hydrogen peroxide, *Environ. Eng. Sci.*, 33 (2016) 185–192.
- [8] Z.H. Jiang, Technical progress and market demand of pyridine compounds, acetaldehyde acetic acid, *Chem. Ind.*, 1 (2013) 14–17.
- [9] D.R. Stapleton, I.K. Konstantinou, D. Mantzavinos, D. Hela, M. Papadaki, On the kinetics and mechanisms of photolytic/ $TiO_2$ -photocatalytic degradation of substituted pyridines in aqueous solutions, *Appl. Catal., B.*, 95 (2010) 100–109.
- [10] F. Tian, R. Zhu, F. Ouyang, Synergistic photocatalytic degradation of pyridine using precious metal supported  $TiO_2$  with  $KBrO_3$ , *J. Environ. Sci.*, 11 (2013) 2299–2305.
- [11] S.V. Mohan, S. Sistla, R.K. Guru, K.K. Prasad, C.S. Kumar, S.V. Ramakrishna, P.N. Sarma, Microbial degradation of pyridine using *Pseudomonas* sp. and isolation of plasmid responsible for degradation, *Waste Manage.*, 23 (2003) 167–171.
- [12] X. Liu, Y. Chen, X. Zhang, X. Jiang, S. Wu, J. Shen, X. Sun, J. Li, L. Lu, L. Wang, Aerobic granulation strategy for bioaugmentation of a sequencing batch reactor (SBR) treating high strength pyridine wastewater, *J. Hazard. Mater.*, 295 (2015) 153–160.
- [13] M.Z. Kamrath, R.A. Relph, M.A. Johnson, Vibrational predissociation spectrum of the carbamate radical anion,  $C_5H_5N-CO_2^-$ , generated by reaction of pyridine with  $(CO_2)_m^-$ , *J. Am. Chem. Soc.*, 132 (2010) 15508–15511.
- [14] O.A. Zalat, M.A. Elsayed, A study on microwave removal of pyridine from wastewater, *J. Environ. Chem. Eng.*, 1 (2013) 137–143.
- [15] F. Nerud, P. Baldrian, J. Gabriel, D. Ogbeifun, Decolorization of synthetic dyes by the Fenton reagent and the Cu/pyridine/ $H_2O_2$  system, *Chemosphere*, 44 (2001) 957–961.
- [16] K.V. Padoley, S.N. Mudliar, S.K. Banerjee, S.C. Deshmukh, R.A. Pandey, Fenton oxidation: a pretreatment option for improved biological treatment of pyridine and 3-cyanopyridine plant wastewater, *Chem. Eng. J.*, 1 (2011) 1–9.
- [17] Q. Zhu, G.D. Moggridge, C. D'Agostino, Adsorption of pyridine from aqueous solutions by polymeric adsorbents MN 200 and MN 500. Part 2: kinetics and diffusion analysis, *Chem. Eng. J.*, 306 (2016) 1223–1233.
- [18] D. Li, J. Tang, X. Zhou, J. Li, X. Sun, J. Shen, L. Wang, W. Han, Electrochemical degradation of pyridine by  $Ti/SnO_2$ -Sb tubular porous electrode, *Chemosphere*, 149 (2016) 49–56.
- [19] S. Kumar, S. Singh, V.C. Srivastava, Electro-oxidation of nitrophenol by ruthenium oxide coated titanium electrode: parametric, kinetic and mechanistic study, *Chem. Eng. J.*, 263 (2015) 135–143.
- [20] C.W. Zhu, C.Q. Jiang, S. Chen, R.Q. Mei, X. Wang, J. Cao, L. Ma, B. Zhou, Q.P. Wei, G.Q. Ouyang, Z.M. Yu, K.C. Zhou, Ultrasound enhanced electrochemical oxidation of Alizarin Red S on boron doped diamond(BDD) anode: Effect of degradation process parameters, *Chemosphere*, 209 (2018) 685–695.
- [21] A. Fajardo, H. Seca, R. Martins, V. Corceiro, I. Freitas, M. Quinta-Ferreira, R. Quinta-Ferreira, Electrochemical oxidation of phenolic wastewaters using a batch-stirred reactor with NaCl electrolyte and  $Ti/RuO_2$  anodes, *J. Electroanal. Chem.*, 785 (2016) 180–189.
- [22] E. Isarain-Chávez, M.D. Baró, E. Rossinyol, U. Morales-Ortiz, J. Sort, E. Brillas, E. Pellicer, Comparative electrochemical oxidation of methyl orange azo dye using  $Ti/Ir-Pb$ ,  $Ti/Ir-Sn$ ,  $Ti/Ru-Pb$ ,  $Ti/Pt-Pd$  and  $Ti/RuO_2$  anodes, *Electrochim. Acta*, 244 (2017) 199–208.
- [23] K.D. Radosavljević, J.D. Lović, D.Ž. Mijin, S.D. Petrović, M.B. Jadranić, A.R. Mladenović, M.L. Avramov Ivić, Degradation of azithromycin using  $Ti/RuO_2$  anode as catalyst followed by DPV, HPLC–UV and MS analysis, *Chem. Pap.*, 71 (2017) 1217–1224.
- [24] P.J. Kuang, C.P. Feng, N. Chen, W. Hu, G. Wang, T. Peng, L. Lv, Improvement on electrochemical nitrate removal by combining with the three-dimensional (3-D) perforated iron cathode and the iron net, *J. Electrochem. Soc.*, 163 (2016) 397–406.
- [25] H.Y. Li, X. Xing, K. Wang, X.P. Zhu, Y. Jiang, J.X. Xia, Improved BDD anode system in electrochemical degradation of p-nitrophenol by corroding electrode of iron, *Electrochim. Acta*, 291 (2018) 335–342.
- [26] M. Ali, A. Elreedy, M.G. Ibrahim, M. Fujii, A. Tawfik, Hydrogen and methane bio-production and microbial community dynamics in a multi-phase anaerobic reactor treating saline industrial wastewater, *Energy Convers. Manage.*, 186 (2019) 1–14.
- [27] X.H. Chen, Rapid detection of 39 carbamate pesticide residues in drinking water by liquid chromatography-tandem mass spectrometry, *Ecol. Environ. Monit. Three Gorges*, 3 (2018) 55–61.
- [28] S.L. Ferreira, R.E. Bruns, H.S. Ferreira, G.D. Matos, J.M. David, G.C. Brando, E.G. da Silva, L.A. Portugal, P.S. dos Reis, A.S. Souza, W.N. dos Santos, Box–Behnken design: an alternative for the optimization of analytical methods, *Anal. Chem. Acta*, 597 (2007) 179–186.
- [29] E. Flores-Girón, J.A. Salazar-Montoya, E.G. Ramos-Ramírez, Application of a Box–Behnken design for optimizing the extraction process of agave fructans, *J. Sci. Food Agric.*, 96 (2015) 3860–3866.
- [30] S. Choe, H.M. Liljestrand, J. Khim, Nitrate reduction by zero-valent iron under different pH regimes, *Appl. Geophys.*, 19 (2004) 335–342.
- [31] X.Y. Duan, F. Xu, Y.N. Wang, Y.W. Chen, L.M. Chang, Fabrication of a hydrophobic SDBS- $PbO_2$  anode for electrochemical degradation of nitrobenzene in aqueous solution, *Electrochim. Acta*, 282 (2018) 662–671.
- [32] Z. Xu, H. Liu, J. Niu, Y. Zhou, C. Wang, Y. Wang, Hydroxyl multi-walled carbon nanotube-modified nanocrystalline  $PbO_2$  anode for removal of pyridine from wastewater, *J. Hazard. Mater.*, 327 (2017) 144–152.
- [33] P.J. Kuang, C.P. Feng, M. Li, N. Chen, Q. Hu, G. Wang, R. Li, Improvement on electrochemical reduction of nitrate in synthetic groundwater by reducing anode surface area, *J. Electrochem. Soc.*, 164 (2017) 103–112.
- [34] B. Khemakhem, I. Fendri, I. Dahech, K. Belghuith, R. Kammoun, H. Mejdoub, Purification and characterization of a maltogenic amylase from Fenugreek (*Trigonella foenum graecum*) seeds using

- the Box–Benken Design (BBD), *Ind. Crops Prod.*, 43 (2013) 334–339.
- [35] Y. Deng, N. Chen, C. Feng, F. Chen, H. Wang, P. Kuang, Z. Feng, T. Liu, Y. Gao, W. Hu, Treatment of organic wastewater containing nitrogen and chlorine by combinatorial electrochemical system: taking biologically treated landfill leachate treatment as an example, *Chem. Eng. J.*, 364 (2019a) 349–360.
- [36] Y. Deng, N. Chen, C. Feng, H. Wang, Y. Zheng, F. Chen, W. Lu, P. Kuang, H. Feng, Y. Gao, W. Hu, Degradation of nitrogen-containing refractory organic wastewater using a novel alternating-anode electrochemical system, *Sci. Total Environ.*, 697 (2019b) 134161.
- [37] M. Li, C.P. Feng, Z. Zhang, S. Yang, N. Sugiura, Treatment of nitrate contaminated water using an electrochemical method, *Bioresour. Technol.*, 101 (2010) 6553–6557.
- [38] Y. Wang, Z. Shen, X. Chen, Effects of experimental parameters on 2,4-dichlorophenol degradation over Er-chitosan-PbO<sub>2</sub> electrode, *J. Hazard. Mater.*, 178 (2010) 867–874.
- [39] J. Du, Z. Chen, C. Chen, T.J. Meyer, An alternative half reaction to water oxidation: chloride oxidation to chlorine catalyzed by silver ion, *J. Am. Chem. Soc.*, 137 (2015) 3193–3196.
- [40] A. Urtiaga, P. Fernandez-Castro, P. Gómez, I. Ortiz, Remediation of wastewaters containing tetrahydrofuran. Study of the electrochemical mineralization on BDD electrodes, *Chem. Eng. J.*, 239 (2014) 341–350.
- [41] E. Brillas, J. Casado, Aniline degradation by electro-Fenton and peroxi-coagulation processes using a flow reactor for wastewater treatment, *Chemosphere*, 47 (2002) 241–248.
- [42] G. Emtiazi, M. Satarii, F. Mazaherion, The utilization of aniline, chlorinated aniline, and aniline blue as the only source of nitrogen by fungi in water, *Water Res.*, 35 (2001) 1219–1224.
- [43] S.P. Kamble, S.B. Sawant, J.C. Schouten, V.G. Pangarkar, The utilization of aniline, chlorinated aniline, and aniline blue as the only source of nitrogen by fungi in water, *J. Chem. Technol. Biotechnol.*, 78 (2003) 865–872.
- [44] J. Jasper, Y. Yang, M.R. Hoffmann, Toxic by-product formation during electrochemical treatment of latrine wastewater, *Environ. Sci. Technol.*, 51 (2017) 7111–7119.
- [45] A. Adachi, H. Hamamoto, T. Okano, Use of lees materials as an adsorbent for removal of organochlorine compounds or benzene from wastewater, *Chemosphere*, 58 (2005) 817–822.
- [46] Y. Zhou, C. Shi, G. Dong, Analysis of a mechanical vapor recompression wastewater distillation system, *Desalination*, 353 (2014) 91–97.
- [47] A. Fernandes, D. Santos, M.J. Pacheco, L. Ciriaco, A. Lopes, Electrochemical oxidation of humic acid and sanitary landfill leachate: influence of anode material, chloride concentration and current density, *Sci. Total Environ.*, 541 (2016) 282–291.
- [48] Y. Deng, C. Feng, N. Chen, W. Hu, P. Kuang, H. Liu, Z. Hu, R. Li, Research on the treatment of biologically treated landfill leachate by joint electrochemical system, *Waste Manage.*, 82 (2018) 177–187.
- [49] J. Zhou, Y. Ding, Experimental study on acid dye wastewater treatment by electrochemical oxidation, *Ind. Water Wastewater*, 6 (2011) 37–39.
- [50] H. Zhang, D. Zhang, J. Zhou, Removal of COD from landfill leachate by electro-Fenton method, *J. Hazard. Mater.*, 135 (2006) 106–111.
- [51] O. Gökhan, H. Gökçe, K. Özgül, Application of response surface methodology (RSM) to evaluate the influence of deposition parameters on the electrolytic Cu-Zn alloy powder, *Int. J. Electrochem. Sci.*, 6 (2011) 3966–3981.
- [52] A. Fernandes, M.J. Pacheco, L. Ciriaco, A. Lopes, Review on the electrochemical processes for the treatment of sanitary landfill leachates: present and future, *Appl. Catal., B*, 176–177 (2015) 183–200.
- [53] P. Kuang, N. Chen, C. Feng, M. Li, S. Dong, L. Lv, J. Zhang, Z. Hu, Y. Deng, Construction and optimization of an iron particle–zeolite packing electrochemical–adsorption system for the simultaneous removal of nitrate and by-products, *J. Taiwan Inst. Chem. Eng.*, 86 (2018) 101–112.
- [54] A.R. Rahmani, K. Godini, D. Nematollahi, G. Azarian, Electrochemical oxidation of activated sludge by using direct and indirect anodic oxidation, *Desal. Water Treat.*, 56 (2015) 2234–2245.
- [55] F. Khasaeva, N. Vasilyuk, P. Terentyev, M. Troshina, A.T. Lebedev, A novel soil bacterial strain degrading pyridines, *Environ. Chem. Lett.*, 9 (2011) 439–445.
- [56] L. Zhang, R. Tian, Z. Chen, J. Guo, Y. Jia, Effects of NaCl salinity on wastewater pollutants removal and microorganism in A<sup>2</sup>/O technology process, *Trans. Chin. Soc. Agr. Eng.*, 34 (2018) 231–237.